ANALYSIS OF TWO-DIMENSIONAL INCOMPRESSIBLE FLOW PAST AIRFOILS USING UNSTEADY NAVIER-STOKES EQUATIONS†

BY

K.N. Ghia, G.A. Osswald and U. Ghia*

Department of Aerospace Engineering and Engineering Mechanics
*Department of Mechanical Engineering
University of Cincinnati
Cincinnati, Ohio

Abstract

The conservative form of the unsteady Navier-Stokes equations in terms of vorticity and stream function in generalized curvilinear coordinates are used to analyze the flow structure of steady separation and unsteady flow with massive separation. The numerical method solves the discretized equations using an ADI-BGE method. The method is applied to a symmetric 12 percent thick Joukowski airfoil. A conformal clustered grid is generated; several 1-D stretching transformations are used to obtain a grid that attempts to resolve many of the multiple scales of the unsteady flow with massive separation, while maintaining the transformation metrics to be smooth and continuous in the entire flow field. Detailed numerical results are obtained for three flow configurations (i) Re = 1000, α = 5°, (ii) Re = 1000, α = 15°, (iii) Re = 10,000, α = 5°. No artificial dissipation was added; however, lack of a fine grid in the normal direction has presently led to results which are considered qualitative, especially for case (iii).

1. Introduction

The flow over streamlined lifting airfoils has been a subject of considerable interest to fluid dynamicists and, to date, significant progress has been made towards the design of airfoils, wings, etc., by drawing together resources from experimental, numerical, analytical and empirical studies. The detailed flow structure of airfoils and wings near maximum lift in low-to-high Reynolds number (Re) flows still remains unresolved. The increasing interest in these flows stems from the desire for better control in civilian aircraft, to high maneuvering capability in high-performance military aircraft. The improved performance can be realized from the potential of increasing maximum lift and simultaneously reducing drag under this condition. For some combination of flow parameters, the flow field around an airfoil experiences significant separation which deteriorates its performance and leads to the stall phenomenon. The nature of the stall may be characterized by the various phenomena such as separation, unsteadiness, transition and turbulence. The present study is directed towards accurately simulating this flow field and providing further insight for this class of flows. Other important fluid dynamics applications involving unsteady flows include blade rows in turbomachinery, marine propellers, helicopter rotor blades, and bluff bodies such as buildings, towers, underwater cables, etc., in cross flows. For this class of bluff-body flows, understanding the vortex shedding characteristics is very significant. The simulation technique presented here can also provide guidelines for analyzing some of these flow fields.

For two-dimensional, incompressible, unsteady, viscous, separated flows at moderately high Reynolds number, two viable approaches are available. (i) The first method involves an inviscid-viscous strong-interaction analysis based on localized-flow regions, whereas (ii) the second method consists of using, in the entire region of interest, a single set of equations which have the necessary mutual dependence between the inviscid and viscous flow built into them. For massive separated viscous unsteady flows of interest in this study, the second approach is preferred. In this latter approach, the complete unsteady Navier-Stokes equations are preferred over other reduced forms of Navier-Stokes equations discussed by K. Ghia, Osswald and U. Ghia [1].

The prediction of two-dimensional flow past various airfoils has been comprehensively reviewed by Cebeci, Stewartson and Whitelaw [2]. Noteworthy papers on both the computational approaches mentioned earlier, as well as experimental and analytical methods, have been extensively reviewed by these authors and as such, no attempt is made here to review the past work. Instead, only some relevant studies using the Navier-Stokes equations approach and a couple of very recent experimental and analytical studies are cited here. Mehta and Lavan [3] studied the incompressible flow past a 9 percent thick Joukowski airfoil at Re = 1000, and angle of incidence, α = 15°, using the Navier-Stokes equations, and provided accurate results for the stall characteristics. Care was exercised in determining the far-field boundary condition which was placed at a finite distance from the airfoil. Their numerical simulation employed an O-type grid; the resolution of an O-grid generally degrades in the wake region. The dynamic stall of an

† This research was supported, in part, by NASA Grant No. NAG-1-465 and, in part, by AFOSR Grant No. 80-0160.

oscillating airfoil was also studied by Mehta [4] using the Navier-Stokes equations for the NACA 0012 airfoil with Re up to 10,000 and the reduced frequency of oscillation k = 0.5 based on the half-chord. The formation of the leading-edge vortex was carefully simulated using a fourth-order accurate method, again, with the O-grid. Wu and his coworkers [5] have contributed significantly in developing integro-differential and integral methods for the solution of the Navier-Stokes equations for incompressible and compressible, as well as laminar and turbulent, flows past Joukowski airfoils at angle of attack. In some of these studies, flow past a 9 percent thick symmetric Joukowski airfoil at Re = 1000 and $\alpha = 15°$ was computed. In order to improve the efficiency of their solution, Wu et al. [6] suggested a zonal procedure with the unique feature of using the complete unsteady Navier-Stokes equations only in the massive separated detached zone. For the same Joukowski airfoil configuration, they showed improved computational efficiency. Hodge et al. [7] solved the unsteady Navier-Stokes equations using O-grids and predicted flows around NACA airfoils at stall Re of 4×10^4 and 2×10^5 and compared their results qualitatively with experimental data.

Mueller [8] experimentally studied the Lissaman 7769 and Miley M06-13-128 airfoils at Re < 300,000 which is lower than their design value of Re = 600,000. A hysteresis loop was observed which depended on the relative locations of laminar separation and transition. This data may become valuable for validating numerical analysis for these airfoils. Smith [9] has reviewed the theoretical aspects of steady and unsteady laminar separation. The importance of a rational theoretical analysis in building a basis for the interacting-analysis approach and providing guidelines in the resolution of multiple scales by properly developing the grid for the Navier-Stokes approach was clearly emphasized. The two-dimensional unsteady separation was linked closely with instabilities in the boundary layer and the separating shear layer. It is the belief of the present authors that coherent experimental, theoretical and numerical studies, with proper interaction amongst them, are needed to gain a more complete understanding of unsteady separated flows.

The primary objective of the present work is to study the two-dimensional unsteady separated flow past an airfoil at moderate Re near the stall conditions and accurately determine the flow characteristics in the massive separated region. To achieve this goal, the analysis of K. Ghia, Osswald and U. Ghia [1] developed earlier for internal flow was used as the starting basis for analyzing the flow past symmetric Joukowski airfoils at high angle of attack.

2. Governing Equations

In terms of the vorticity vector $\bar{\omega}$ and the velocity vector $\bar{V}$, the unsteady, incompressible Navier-Stokes equations consist of a temporally parabolic vorticity transport equation

$$\frac{\partial\bar{\omega}}{\partial t} + (\bar{V}\cdot\nabla)\bar{\omega} = (\bar{\omega}\cdot\nabla)\bar{V} - \frac{1}{Re}(\nabla\times\nabla\times\bar{\omega}) \qquad (1)$$

together with the kinematic definition for vorticity

$$\bar{\omega} = \nabla\times\bar{V} \quad . \qquad (2)$$

Here, Re is a Reynolds number defined as

$$Re = U_R L_R/\nu = U_\infty C/\nu$$

where, for the airfoil problem, the reference speed U_R is U_∞, the reference length L_R is the chord c and ν is the constant kinematic viscosity of the incompressible fluid. Equations (1) and (2) have been nondimensionalized using c as the characteristic unit of length, U_∞ as the characteristic unit of speed, c/U_∞ as the characteristic unit of time, and U_∞/c as the characteristic unit of vorticity.

For 2-D or axisymmetric flow, the local velocity vector $\bar{V}$ can be related to a stream function ψ as

$$\bar{V} = \nabla\psi\times\bar{e}^3 \qquad (3)$$

where $\bar{e}^3$ is the fundamental contravariant base vector. For consistency with Eqs. (1) and (2), Eq. (3) is nondimensionalized using $U_\infty c^2$ as the characteristic unit for ψ.

Equations (1-3) represent a vorticity-stream function formulation for the unsteady, incompressible Navier-Stokes equations. For numerical implementation, their component form in a generalized coordinate system (ξ^1,ξ^2) has been given by Osswald, K. Ghia and U. Ghia [10]. Use of the two-dimensional component form of the equations for ω and ψ in (ξ^1,ξ^2) coordinates, together with appropriate boundary conditions for ω and ψ, leads to a well-posed boundary-value problem for the airfoil flow. However the discussion on the boundary conditions will be deferred until the coordinate system to be used has been selected. The governing equations (1-3) form a coupled set of nonlinear equations and some comments are made next on the numerical method used to obtain their solution.

3. Comments on the Numerical Method

The numerical method used was first developed by Osswald and Ghia [11] and was further refined by K. Ghia, Osswald and U. Ghia [1]. As discussed in Ref. [1], this method can be briefly described as follows. The spatial derivatives are approximated by appropriate finite-difference quotients using central differences for both convective and diffusive derivatives in the governing equations. It is significant to note that, in this study, even with central-difference approximations for all spatial derivatives, no artificial dissipation is added to dampen any high-frequency errors, but continued effort is made to carefully annihilate these errors through appropriate resolution of the various length scales of the problem. For consistent differencing, some of the metric

coefficients are evaluated at the staggered half-grid point locations, whereas the metric determinant, the solution field functions and the source term are evaluated at the cell corners. The conservative form of the vorticity transport equation is solved, using an ADI method, whereas the stream function equation is solved using a block Gaussian elimination (BGE) technique. The BGE technique is a direct extension of the Gaussian elimination method to matrices whose individual elements are themselves matrices or blocks. The BGE technique provides the effective inversion of an (N•M × N•M) matrix through the actual inversion of a predetermined sequence of N(M×M) submatrices; the choice of M<N leads to the best computational efficiency. The BGE approach naturally divides itself into two separate calculation phases. In the first phase, a sequence of N(M×M) matrices is formed and individually inverted by simple scalar Gaussian elimination. This phase is the most time-consuming part of the calculation. Fortunately, this preliminary phase need be executed only once for a given coordinate choice, its result being permanently stored as a series of coefficient matrices for later use in the second phase of this procedure. The second phase consists of the actual solution of the block matrix problem for a prescribed source term through a set of recursion relationships. In this method, the transport equation at time level t_{n+1} is discretized with the stream function being frozen at the time level t_n. Due to this uncoupling, the formal temporal accuray of the scheme is $O(\Delta t_n)$ with the overall formal truncation accuracy of $O[\Delta t_n, (\Delta\xi^1)^2, (\Delta\xi^2)^2]$. For solution of the unsteady Navier-Stokes equations, it is the Dirichlet stream-function Poisson problem which must be solved repeatedly in a given coordinate system for a progression of updated sources. Hence, the combined ADI-BGE method used here is very well suited for analyzing incompressible unsteady separated flows governed by the unsteady Navier-Stokes equations.

4. Massive Separated Incompressible Flow Past Symmetric Joukowski Airfoils

The flow past a 12 percent thick symmetric Joukowski airfoil at moderate Re separates when the free stream is at incidence to the airfoil. As the angle of attack is increased, even at moderate Re, a region of massive separation develops on the upper surface. The geometry of the model problem of flow past a Joukowski airfoil can be accurately represented using conformal transformation techniques (see, e.g., Davis [12] and Ives [13]), and various conformal grids have been obtained for this problem. Furthermore, the flow past a Joukowski airfoil has been used by many investigators as a model problem for studying viscous separated flow, because of the simplicity of its geometry for this class of flows. Consequently, results of other investigators are also available for qualitative comparison and, hence, this problem is used as a model problem in the present study.

4.1 The Coordinate System

Clustered conformal coordinates are employed in the present viscous-flow study. These coordinates are obtained by a parabolic transformation of the inviscid-flow complex-potential plane, followed by appropriate 1-D clustering transformations for resolving the various length scales of the flow problem.

For lifting cases, i.e., for flows past airfoils at non-zero incidence α, the corresponding inviscid flow has non-zero circulation Γ and, consequently, a multi-valued potential function Φ_{in}. Also, the inviscid flow is not symmetric about the airfoil mean line or camber line. Nevertheless, all of the viscous-flow results presented in this paper for symmetric airfoils were obtained using a coordinate system which is symmetrical about the airfoil chord line, even for the lifting cases. In other words, the coordinates used are based on the corresponding potential flow with zero circulation and are obtained as a limiting case of the general coordinates developed for the inviscid flow with non-zero circulation. Some details of generating these general conformal coordinates for flows with circulation are described here in this section. For additional details, see Osswald, K. Ghia and U. Ghia [14]. The use of these general coordinates in the study of viscous flows for lifting airfoils will be the subject of a future paper.

4.1.1 Inviscid Flow Past a Joukowski Airfoil at Incidence

The complex potential P for the inviscid flow of a uniform stream at incidence α past a symmetric Joukowski airfoil is obtained conveniently from the knowledge of the complex potential for flow past a circular cylinder into which the Joukowski airfoil can be mapped via the Joukowski transformation. Accordingly, the complex potential is given as

$$P = R + \frac{a^2}{R} + i\,\frac{\Gamma}{2\pi}\,\ell n\left(\frac{R}{a}\right) \qquad (4)$$

where

$P \triangleq (\Phi_{in} + i\,\Psi_{in})$ is the complex potential,

Φ_{in}, Ψ_{in} are the velocity potential and stream function, respectively, for the 2-D inviscid flow,

$R \triangleq (r^1 + ir^2)$ is the complex variable in the circle plane in which the Joukowski airfoil profile is mapped as a circle,

a is the radius of the circular cylinder in the circle plane,

and

$\Gamma = 4\pi a \sin\alpha$ is the circulation around the cylinder (or airfoil).

The radius a is related to the thickness ratio (i.e. maximum thickness t_{max}/chord c) of the airfoil and the incidence angle α of the free stream approaching the airfoil. This relation is established by the Joukowski transformation as discussed next.

The complex variable R in the circle plane is related to the complex variable z ($\triangleq x^1 + ix^2$) in the physical plane via the Joukowski transformation as

$$z = \tau + \frac{p^2}{\tau} + |z_{LE}| \qquad (5)$$

where

$$\tau = R\, e^{i\alpha} - \varepsilon p \quad ,$$

$$|z_{LE}| = [(1+2\varepsilon) + (\tfrac{1}{1+2\varepsilon})]\, p \quad ,$$

$$p = (1+2\varepsilon)/[1 + (1+2\varepsilon)(3+2\varepsilon)]$$

and ε is related to the thickness ratio t_{max}/c by the expression

$$\frac{4\varepsilon p(1+\varepsilon)^2}{1 + 2\varepsilon(1+\varepsilon)(1-\cos\theta_m)} = \frac{t_{max}}{c}\,[\sin\theta_m(1-\cos\theta_m)] \quad . \tag{6}$$

In this expression, θ_m is the value of θ in the physical plane at which the maximum thickness of the airfoil occurs, i.e.,

$$\theta_m = \theta\big|_{y(\theta)=0.5\, t_{max}/c} \quad .$$

It should be noted that an $O(\varepsilon^2)$ approximate solution to Eq. (6) can be obtained to yield $\theta_m = 2\pi/3$ so that $\varepsilon = \frac{4}{3\sqrt{3}}\frac{t_{max}}{c}$. In the present study, however, this approximation was not invoked, but Eq. (6) was solved numerically using the method of successive substitution. It was observed that, for a 12 percent thick symmetric Joukowski airfoil, the value of ε so determined differed from the approximate value by almost 10 percent.

Figure (1) shows the inviscid flow problem considered in the physical plane, the circle plane and, finally, in the complex-potential plane. The lines of Φ_{in} = constant and Ψ_{in} = constant form a rectangular coordinate system in the P-plane and yield a surface-oriented conformal coordinate system in the physical plane. Hence, the P-plane could constitute the computational plane. However, it is not quite appropriate for this purpose because of the following three main reasons. First of all, the coordinates Ψ_{in} = constant experience large turning in the vicinity of the leading stagnation point, the degree of turning depending upon the incidence angle α and the roundedness of the airfoil in this region and near the leading edge. Also, the manner in which the coordinates are disposed is not conducive to proper resolution in this region. Secondly, the flow occurs over the entire unbounded P-plane extending from $-\infty$ to $+\infty$ along both Φ_{in} and Ψ_{in}; this is computationally impractial. Finally, it is noted that the airfoil profile between the leading stagnation point (LSP) and the trailing edge point (TEU) following the upper contour, i.e., along Ψ_{in}, $\bar{\Psi}_{in} = 0^+$, extends from $\Phi_{in} = 0$ to $\Phi_{in} = \Phi_{TEU}$. Following the lower contour, i.e., along $\bar{\Psi}_{in} = 0^-$, the airfoil profile between LSP and TEL extends from $\Phi_{in} = 0$ to $\Phi_{in} = \Phi_{TEL}$ where

$$\Phi_{TEL} = \Phi_{TEU} - \Gamma \quad . \tag{7}$$

In fact, for each point on the trailing streamline in the physical plane,

$$\Phi_\ell = \Phi_u - \Gamma \quad . \tag{8}$$

This distinction in the values of ϕ_{in} must be maintained for all points along the upper and lower trailing streamlines, downstream of the trailing edge. Hence, a desired grid-point distribution may be assigned only along the upper trailing streamline, for example, while the grid point distribution along the lower trailing streamline is no longer arbitrary, but is constrained by condition (8).

Each of the above three points is addressed as follows. First of all, the P-plane is transformed to yet another plane, namely, the η-plane ($\eta \triangleq \eta^1 + i\eta^2$)using the conformal parabolic transformation

$$(\eta)^2 = P + 2a[\cos\alpha + (\alpha+\pi)\sin\alpha] \quad . \tag{9}$$

In the η-plane, the flow problem occupies only the upper-half plane. Secondly, suitable 1-D clustering transformations are employed to map the upper half of the η-plane to a unit square in the ξ-plane ($\xi \triangleq \xi^1 + i\xi^2$) while also providing resolution of the various streamwise and normal length scales in the flow. The nature of these clustering transformations is as discussed in Ref. [15]. Differences in details are necessitated by facts such as the leading stagnation point LSP no longer coinciding with the leading edge point LE. Finally, the requirement expressed in Eqs. (7) or (8) is implemented in the η-plane by recognizing that, downstream of the trailing edge point,

$$\text{along } \Psi_{in} = 0^+ \quad , \quad P = \Phi_u \quad ,$$

and, along $\Psi_{in} = 0^-$, $P = \Phi_\ell$,

so that

$$(\eta^1_\ell)^2 = (\eta^1_u)^2 - \Gamma \quad . \tag{10}$$

for points downstream of the trailing edge. This implementation is carried over to the ξ-plane as well. The ξ-plane constitutes the final computational plane. Use of a uniform mesh in the unit square in the ξ-plane provides a surface-oriented mesh in the unbounded physical plane, with appropriately clustered grid-point distributions. Figure 1(d-e) shows the flow problem represented in the η-plane and finally, in the ξ-plane.

The procedure described in this section was used to generate clustered conformal coordinates for analysis of viscous flow past a 12 percent thick (i.e., $t_{max}/c = 0.12$) Joukowski airfoil. Figure 2(a) shows the coordinate system corresponding to a (229 x 45) mesh for a free stream at zero incidence, i.e., $\alpha = 0$, while Fig. 2(b) shows the coordinates for the case with $\alpha = 10°$. Clustering of coordinate lines can be observed in the region near the airfoil surface as well as near the leading and trailing edges and the leading stagnation point.

4.2 Initial and Boundary Conditions

The final working variables in the flow-problem are the vorticity ω and the perturbation stream function ψ_p defined as the departure of the actual viscous-flow stream function ψ from the corresponding inviscid solution Ψ_{in}, i.e.

$$\psi_p = \psi - \Psi_{in} . \qquad (11)$$

The initial conditions used for the unsteady solution correspond to the requirement that inviscid flow prevails everywhere at the starting time instant T = 0.

The boundary conditions used correspond to the condition of zero slip at the airfoil surface, inviscid-flow conditions infinitely far from the airfoil and continuity of the flow solution across the branch cut along the trailing streamline in the wake. The actual numerical form of the second-order vorticity boundary condition used at the surface is given in Ref. [1]. As in the previous studies by the authors, implicit treatment of all boundary conditions is emphasized. This is maintained for the branch-cut boundary as well.

5. Results and Discussion

5.1 Physical Scales

The unsteady Navier-Stokes analysis and solution procedure discussed in the earlier sections are applied to a 12 percent thick symmetric Joukowski airfoil at moderate Re and angle of incidence α. The steady separated or the unsteady massive separated flow fields over the Joukowski airfoil at angle of incidence have multiple disparate length and time scales. If the physics of this class of flow problems has to be accurately modelled, then these scales must be resolved; otherwise, the flow field will not be simulated accurately in critical areas such as near the separation and reattachment points, etc. Rothmayer and Davis [16] have discussed how the lack of proper resolution of the length scale at the separation point could rather drastically influence the overall eddy and the reattachment point if there is one. Based on whether the separation is mild or massive, two distinct flow structures result. For the former, the viscous layer is of $O(\bar{t}/c)$, where $\bar{t}$ is the thickness of the airfoil, whereas, for the latter case, the detached zone is of O(1). Some of the important length scales associated with these flow structures are the boundary-layer scale of $O(Re^{-1/2})$, the separation scales of $O(Re^{-3/8})$ and $O(Re^{-5/8})$ in the streamwise and normal directions, respectively, at the separation point. Further, since the boundaries external to the body are at true infinity, the inviscid scale of O(u) must be resolved so that the flow smoothly asymptotes to the inviscid boundary conditions. In order to follow the vortices in the wake region, the length scale of the wake region must be resolved. For the unsteady flow field, the temporal scale based on the highest critical frequency needs to be resolved. In the scope of the present study, the scale based on the frequency of the self-induced unsteadiness generated by the shedding of vortices must be resolved. Only if all of the scales mentioned are properly considered in the generation of the grid is there a hope of simulating physical phenomena using the unsteady Navier-Stokes equations.

5.2 Quality of Grid, Accuracy and Computational Efficiency

This discussion on the physical scales shows large disparity in the various scales. This places a major burden on the grid. The conformal clustered grid shown in Fig. 2(a,b) has different clustering transformations on the upper and lower surfaces of the airfoil in the streamwise direction and a different clustering in the wake. Two distinct normal transformations are used both on the upper and lower surfaces. The transformation metrics are smooth and their continuity is maintained across the various regions. Even after exercising this care, a (229×45) computational grid was considered necessary; it uses up the full core capacity of the present host AMDAHL 470 V/7A and Perkin Elmer 3250 MPS computer systems. Hence, the standard approach of refining the grid is not feasible since computational resources do not permit it. Therefore, the results of this study, at present, are considered only qualitative. Every effort is made to prevent them from being contaminated by numerical dissipation or quality of grid; but only after thorough comparison with experimental or asymptotic studies can their quantitative usefulness be assessed. Even in the present work, the analysis was checked for consistancy by using the free-stream condition at all boundaries and ensuring the solution recovered the free-stream values everywhere. It is anticipated that the use of the general conformal clustered grid, discussed in section 4.1, for which the wake centerline approaches the free stream direction will enhance the accuracy of the results.

The use of central differences throughout the flow field leads to the formal overall accuracy of $O[\Delta t, (\Delta\xi^1)^2, (\Delta\xi^2)^2]$. For the configurations with Re = 1000, the resulting solutions are wiggle-free; however, for the case of Re = 10,000, the inadequacy of the grid leads to some oscillations in the vorticity; these are presently being examined. The relative computational efficiency of the present algorithm was measured in terms of the CPU time τ required to advance the solution by one time step per spatial grid point. The value of the "computational effort" index is $\tau = 3.72 \times 10^{-4}$ seconds for the AMDAHL 470 V/7A computer.

5.3 Mildly Separated Steady Flow: Re = 1000, $\alpha = 5^o$

The flow past a symmetric Joukowski airfoil with the parameters listed was computed starting from the inviscid solution shown in Fig. 3(a) at the characteristic time of T = 0. This, as well as, the other results to follow, have been computed using a coordinate system which is symmetrical about the airfoil chord line and is shown in Figure 3(b). The transient stream function and vorticity contours leading to steady state are shown in Fig. 3(c-ℓ). At T = 1.92, in Fig. 3(e), a small separation bubble has been established near the trailing edge (TE). This primary bubble bursts, and the shear layer detaches, with a simultaneous emergence of a secondary bubble at the TE, as seen in Fig. 3(g). The secondary bubble intensifies and

grows and merges with the primary bubble as seen in Fig. 3(i). This configuration achieves steady state around T = 7, but the calculations were continued up to T = 13, Fig. 3(k), by which time it became certain that steady state has been achieved. The vorticity contours show a maximum vorticity of 296 at T = 0.4, Fig. 3(d); the maximum vorticity gradually reduces to 222 at T = 13.0, Fig. 3(ℓ). The vorticity contours show laminar boundary layers on the upper and lower surfaces with a tongue-like behavior in the vorticity at T = 1.92 in Fig. 3(f) and at subsequent times. As time progresses, an asymmetry developes in the vorticity contours and it appears that the region of concentrated vorticity near the leading edge (LE) has been satisfactorily resolved.

5.4 Massive Separation - Unsteady Flow: Re = 1000, α = 15°

Although the present results are obtained as the solution of the unsteady Navier-Stokes equations, the point of flow separation has been defined as the point on the airfoil surface where the surface shear vanishes and the instantaneous streamline detaches from the solid wall. (For further details regarding the separation point in unsteady flow, the reader is referred to the review article by McCrowskey [17]). For the flow configuration discussed in this subsection, results from T = 10.0 to T = 21, extending up to two chord lengths in the wake region, are shown in Fig. 4(a-f). Results beyond the characteristic time of T = 21, not shown here, confirm that the flow is inherently unsteady due to the vortex shedding mechanism established by the free shear-layer instability. The instantaneous stream function contours at T = 10 show massive separation on the suction surface. The shear layer detaches near the LE and never reattaches to the airfoil surface. Two counterclockwise co-rotating bubbles appear aft of the shoulder towards the TE. These bubbles are in the process of coalescing. The corresponding instantaneous vorticity contours show several well developed eddies, some of which are in the process of merging due to intense interaction between them. Intermediate solutions are needed to explain the evolution process of the various eddies and the collective interaction phenomenon described by Ho et al. [18], where more than two eddies merge to form a single eddy. The flow field is dominated by large vortices and their passage over the upper surface produces unsteady forces that are different from those observed during static stall. Following Smith [9], Rothmayer and Davis [16] have referred to this phenomenon as 'dynamic stall'. The large-scale organized structure observed needs further examination in order to seek its relation, if any, to turbulent coherent structure (see Hussain [19]). Figure 4(c) shows the emergence of a new bubble on the suction surface and the previous bubbles in Fig. 4(a) appear to have merged and convected downstream. The corresponding vorticity contours at T = 11 are shown in Fig. 4(d) and are characterized by very similar vortical structures as in Fig. 4(b). At T = 21, the flow structure in Fig. 4(e-f) resembles that in Fig. 4(c-d).

For this configuration, the results are also plotted over a wider field extending up to five chord lengths in the wake region and are shown in Fig. 5(a-d) at the characteristic times T = 11 and 21. The massive separated unsteady flow field is clearly seen here in Fig. 5(a-c). In Fig. 5(c), the shear layer that detaches near LE reattaches at the TE. It is important that instantaneous coefficients of lift and drag be calculated and correlaton with streamline contours be established to show the increase in lift coefficient that may result due to the reattachment of the shear layer at the TE. Figure 5(b-d) shows several vortices interacting with each other. Some fragmentation of lage-scale eddies into small eddies can also be observed. Further analysis of the results for this case reveals a nonlinear limit-cycle type behavior which is presently being quantified, so as to determine, for instance, the Strouhal number for vortex shedding process.

The velocity vectors and pressure coefficient C_p for the two Joukowski airfoil configurations studie at Re = 1000 are depicted in Fig. 6(a-d). For the case of α = 5°, steady-state velocity profiles at various locations on the airfoil and in the wake are shown in Fig. 6(a). These profiles clearly show the mildly separated region as well as the velocity deficit in the wake region. The inviscid as well as the viscous C_p are shown in Fig. 6 (b); the maximum difference between them occurs on the suction surface, very close to the LE, with the magnitude of the inviscid C_p being considerably larger than that of the viscous C_p, as expected. For the unsteady massive separated flow case, instantaneous velocity vectors as well as C_p are shown in Fig. 6(c-d) at T = 21. The velocity profiles show the massive separated region on the airfoil surface; the presence of multiple bubbles in the wake can also be seen by the nature of the wake velocity profiles. The curves of instantaneous C_p show that, for the viscous flow, the leading stagnation point has shifted towards the LE.

The computation of this unsteady flow case with massive separation demonstrates the ability of the analysis to treat the flow past this Joukowski airfoil at higher incidence. Elrafee, Wu and Lekoudis [20] have used a 9 percent thick Joukowski airfoil at Re = 1000, α = 15° and have computed subsonic flow, at M = 0.4 and Pr = 1.0, around it. The results for instantaneous streamline and vorticity contours, as well as the C_p distribution, show rather minimal departure from the corresponding incompressible flow. Further, Sugavanam and Wu [21] have computed turbulent flow past a modified 12 percent thick Joukowski airfoil at Re = 3.6×10^6, α = 15°, using a two-equation k-ε model. The contours of time-averaged streamlines show qualitative resemblance to the contours of instantaneous streamlines shown in Fig. 4, except that the separated region at the high-Re case is smaller in extent. It would be interesting to qualitatively compare the time-averaged vorticity contours with those in Fig. 4; however, these have not been presented by those authors. It should be noted that, in their work, the far-field boundary conditon was placed at approximately eight chord lengths. Detailed examination of other parameters which are more sensitive could perhaps better reveal the departure from the present incompressible unsteady case computed.

5.5 Massive Separation - Unsteady Flow: Re = 10,000, α = 5°

McCroskey [17] has discussed that, when Re > 1000, three-dimensional and turbulence effects are present in the flow field and the unsteady Navier-Stokes analysis should account for these effects. In the present study, this configuration is used to test the ability of the code to compute this flow as well as to find the features distinguishing this flow from that for Re = 1000, even if they are only qualitative, to aid in future study of this phenomenon. As stated earlier, the symmetric grid used is inadequate in the normal direction as well as in the wake, since the wake centerline does not follow the coordinates used. Also, the vorticity contours display some wiggles. Hence, the results for this configuration are, at best, qualitative. Figure 7(a-ℓ) shows the instantaneous stream function and vorticity contours from T = 2.0 to T = 34 for this unsteady flow. At T = 2.0, the instantaneous streamlines in Fig. 7(a) show a well-behaved laminar separated flow. From the corresponding vorticity contours in Fig. 7(b), it appears that the boundary layer is well behaved and a narrow wake trails the airfoil. By T = 5.0, Fig. 7(c), most of the suction surface exhibits reversed flow. Figure 7(d) shows the onset of Tollmien-Schlichting type instability on the upper surface, as well as the emergence and intensification of an eddy near the trailing edge. At present, the available graphics facility is not adequate for post-processing a large-scale data base and only painstaking hard labor has permitted generation of computer plots at some characteristic time instants. With proper graphics facilities which are presently being sought, more precise informaton will be made available in the future. Somewhere between T = 5.0 and T = 12.0, a total breakdown of the flow occurs, with a sudden increase in the normal length scale as can be seen on the suction surface in Fig. 7(f). The streamline contours in the wake at T = 12.0 in Fig. 7(e) are not smooth; this is due to the wiggles that appear in the vorticity field. The wiggles are more prominent on the wake originating from the lower surface and are somewhat reduced as T increases to 14.0, Fig. 7(h), and to subsequent times at T = 24.0 and T = 34, as depicted in Figs. 7(i) and 7(k). The streamline contours at T = 14.0 in Fig. 7(i) bear a strong similarity to those at T = 24.0, suggesting that the flow may exhibit a nonlinear limit-cycle behavior. These qualitative results are encouraging and warrant careful investigation of high-Re flows using this unsteady analysis.

6. Conclusions

The unsteady analysis of Osswald and Ghia [11] has been extended to analyze 2-D unsteady separated external flow past symmetric Joukowski airfoils at high incidence and moderate Re. The boundaries external to the airfoils are placed at infinity. The discretized problem is formulated using central differences for spatial derivatives, thus avoiding any artificial viscosity. The fully implicit ADI-BGE time-marching method, with formal overall accuracy of $O[\Delta t, (\Delta\xi^1)^2, (\Delta\xi^2)^2]$, is used to solve the discretized equations.

Three configurations are investigated for a 12 percent thick Joukowski airfoil and their flow features are carefully discussed. For Re = 1000 and α = 5°, a steady separated flow structure is obtained. For this Re, when α is increased to 15°, a massive unsteady separated flow field is obtained. A nonlinear limit-cycle type analysis is attempted on the latter results. At angle of incidence of 5°, Re was increased to 10,000 and the flow shows an instability around T = 5.0, and exhibits a turbulent-like behavior thereafter. The results of the present analysis are still considered qualitative and fine-mesh results using the new clustered conformal grid (Fig. 2b), are desired in order to make more conclusive statements about the flow structure observed in these results. The results obtained do show the potential of the present analysis to study high-incidence high-Re flow. It is planned to extend the analysis to lifting NACA airfoils and carefully compare the results with available experimental and numerical results.

Acknowledgement

The authors are grateful to Prof. R.T. Davis for his suggestions regarding the generation of conformal grids for lifting airfoils.

References

1. Ghia, K.N., Osswald, G.A. and Ghia, U., (1983), Proceedings of Second Symposium on Numerical and Physical Aspects of Aerodynamic Flows, Long Beach, California.

2. Cebeci, T., Stewartson, K. and Whitelaw, J.H., (1983), Numerical and Physical Aspects of Aerodynamic Flows II, Ed. by T. Cebeci, Springer-Verlag, New York.

3. Mehta, U.B. and Lavan, Z., (1977), Journal of Fluid Mechanics, Vol. 67, Part 2.

4. Mehta, U.B., (1977), Proceedings of AGARD Fluid Dynamics Panel Symposium on Unsteady Aerodynamics, Ottawa, Canada.

5. Wu, J.C., (1982), Chapter 4 of Developments in Boundary Element Methods - 2, Editors: R. Shaw and P. Banerjee, Applied Science Publishers, London.

6. Wu, J.C., Wang, C.M. and Gulcat, U., (1984), AIAA Paper, No. 84-1637.

7. Hodge, J.K., Stone, A.L. and Miller, T.E., (1979), AIAA Journal, Vol. 17, No. 5.

8. Mueller, T.J., (1984), AIAA Paper No. 84-1617.

9. Smith, F.T., (1984), AIAA Paper No. 84-1582.

10. Osswald, G.A., Ghia, K.N. and Ghia, U., (1984), AIAA Paper No. 84-1584.

11. Osswald, G.A. and Ghia, K.N., (1981), Multigrid Methods, NASA CP-2202.

12. Davis, R.T., (1983), Computational Methods for Turbulent, Transonic, and Viscous Flows, Ed. by J.A. Essers, Hemisphere Publishing Co., New York.

13. Ives, D.C., (1982), Numerical Grid Generation, Editor: J.F. Thompson.

14. Osswald, G.A., Ghia, K.N. and Ghia, U., (1985), AFL Report 85-1-169, University of Cincinnati, Cincinnati, Ohio.

15. Ghia, K.N., Osswald, G.A. and Ghia, U., (1984), Proceedings of Theoretical Aerodynamics Conference, Hampton, Virginia.

16. Rothmayer, A.P. and Davis, R.T., (1985), Proceedings of Third Symposium on Numerical and Physical Aspects of Aerodynamic Flows, Long Beach, California.

17. McCroskey, W.J., (1977), Journal of Fluids Engineering, Vol. 99.

18. Ho, C.-M. and Nossier, N.S., (1981), Journal of Fluid Mechanics, Vol. 105.

19. Hussain, A.K.M.F., (1981), Proceedings of Indian Academy of Sciences, Vol. 4, Part 2.

20. Elrafee, M.M., Wu, J.C. and Lekoudis, S.G., (1982), AIAA Journal, Vol. 20, No. 3.

21. Sugavanam, A. and Wu, J.C., (1982), AIAA Journal, Vol. 20, No. 4.

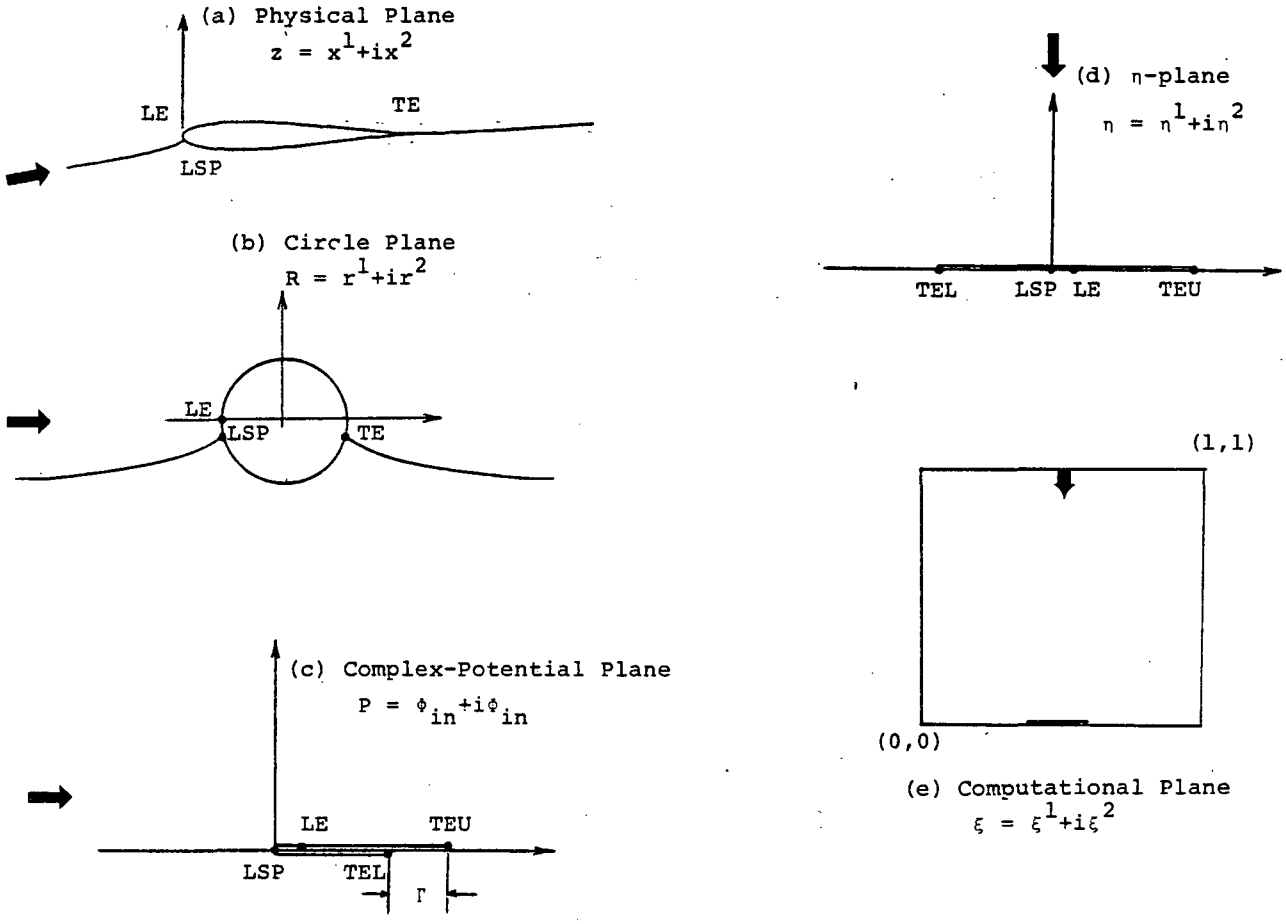

Fig. 1. Representation of Inviscid Flow Past Symmetric Joukowski Airfoil with Circulation, in Physical Plane and Various Transformed Planes.

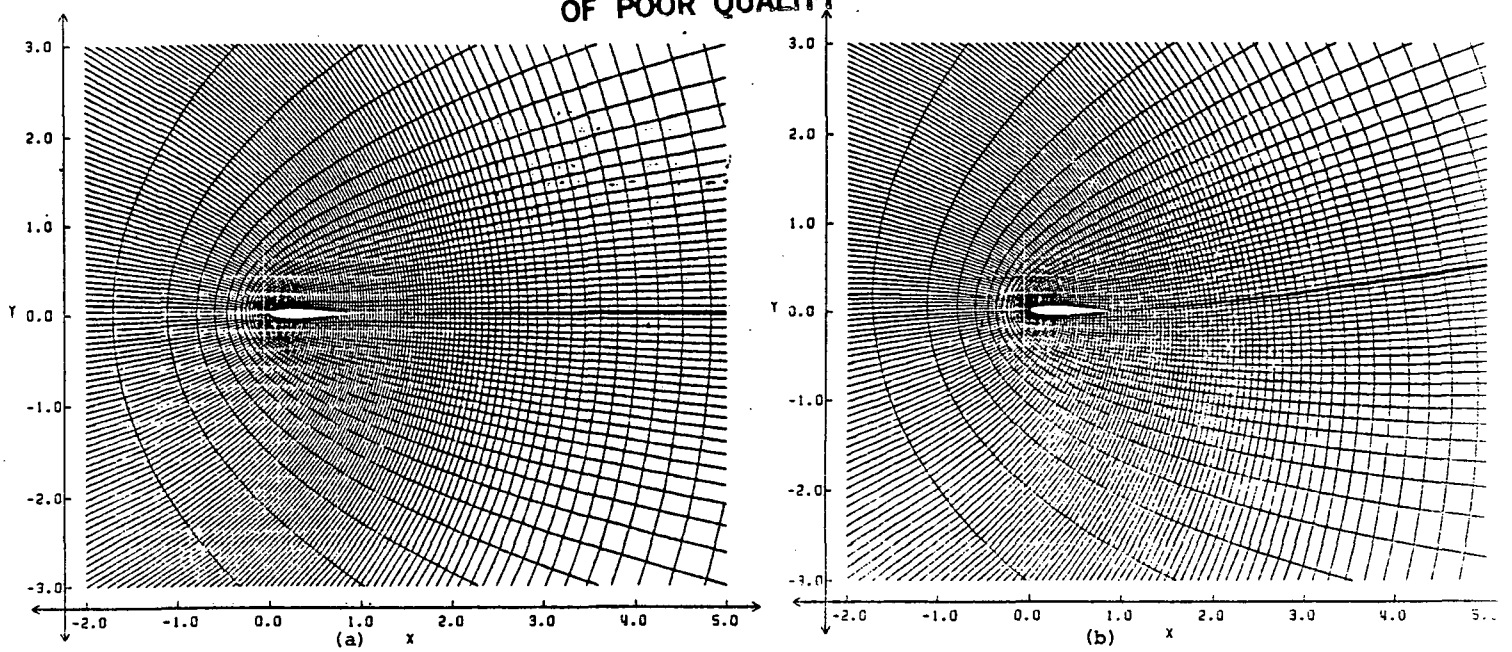

Fig. 2. Coordinate System for Symmetric Airfoil; (a) Zero Incidence; (b) Non-Zero Incidence.

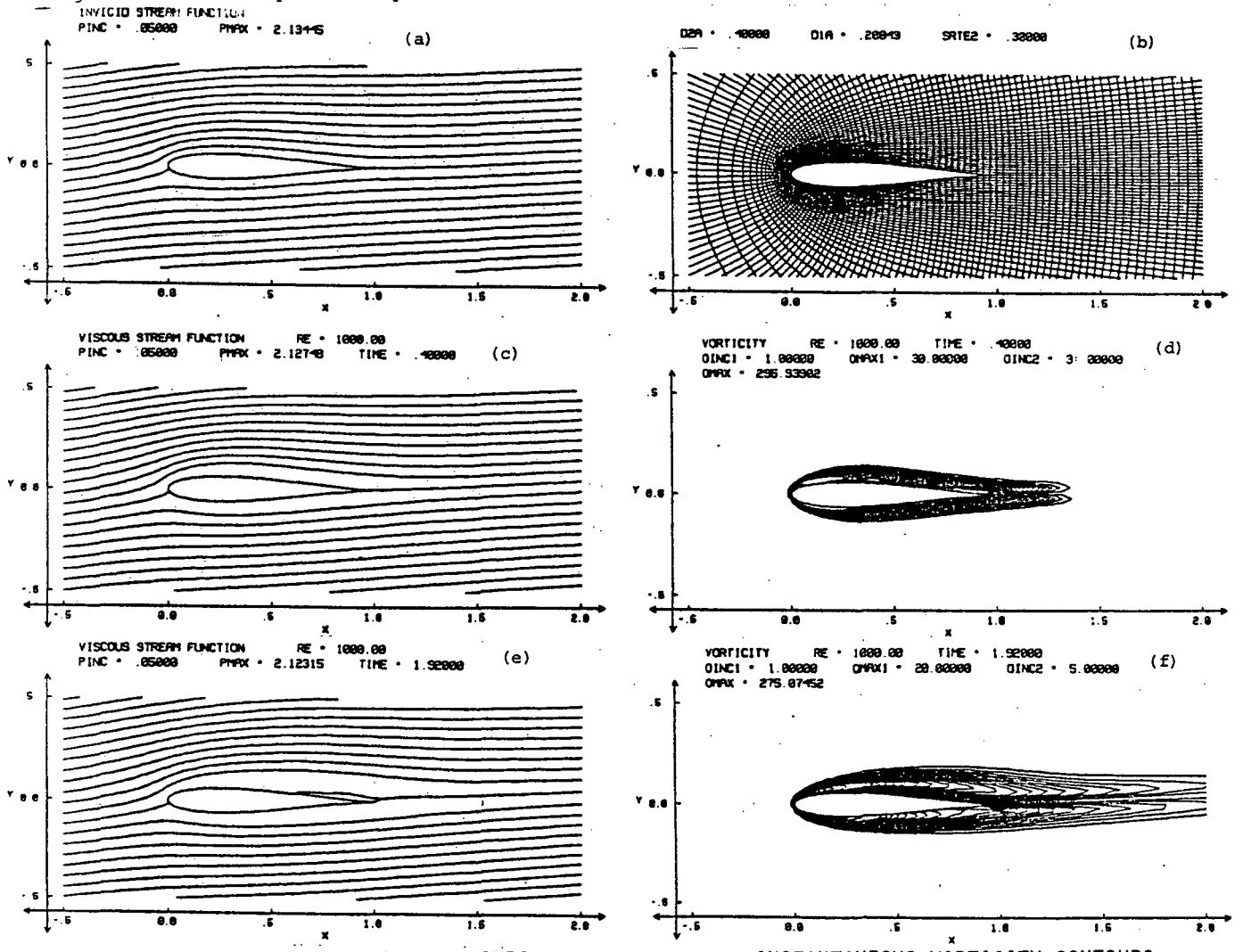

Fig. 3. Flow Past Symmetric Joukowski Airfoil at Re = 1,000, $\alpha = 5°$. T = 0.40 and 1.92.
[At T = 0: Inviscid Stream Function and Grid-Point Distribution]

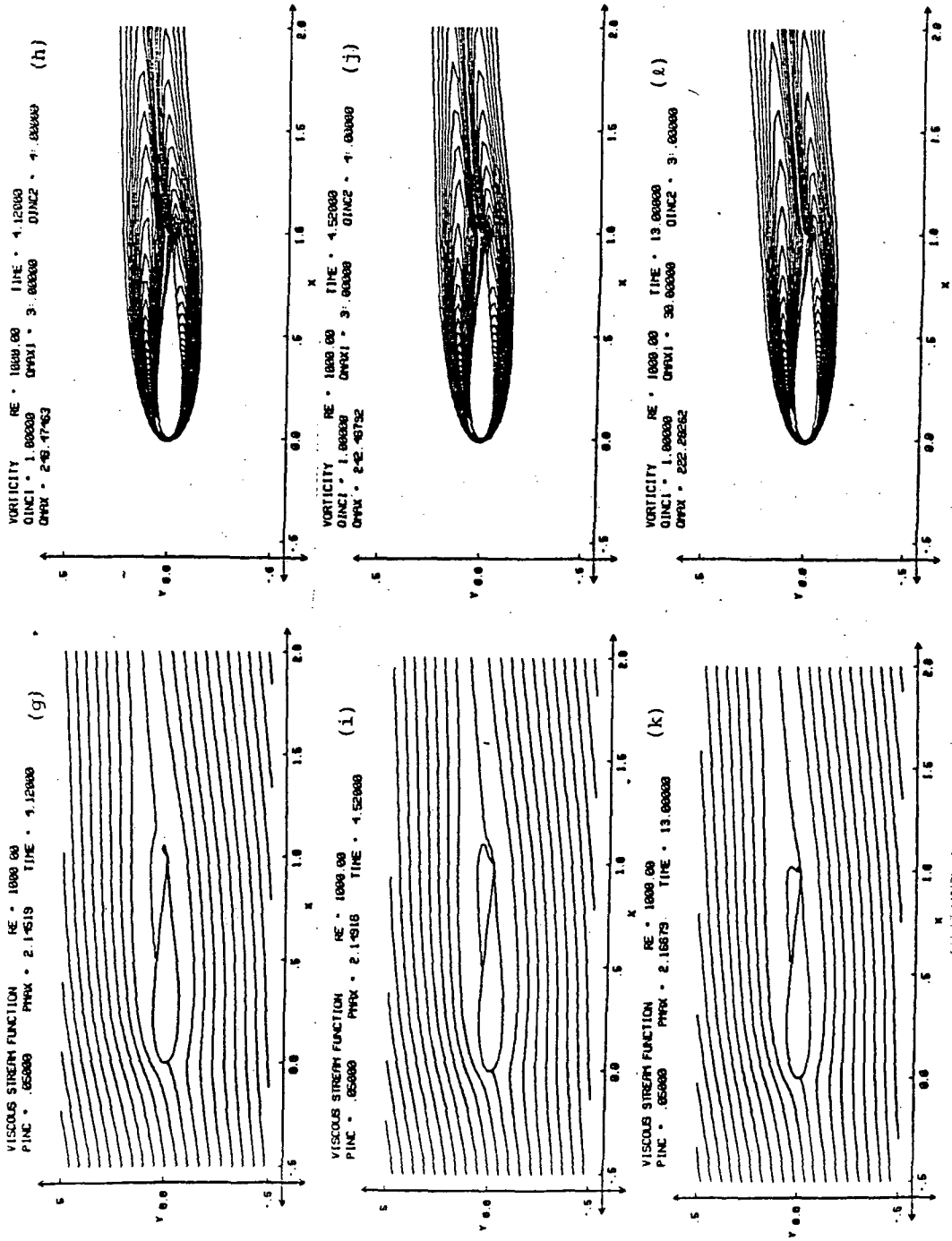

Fig. 3 (Concluded). Flow Past Symmetric Joukowski Airfoil at Re = 1,000, α = 5°. T = 4.12, 4.52, 13.00.

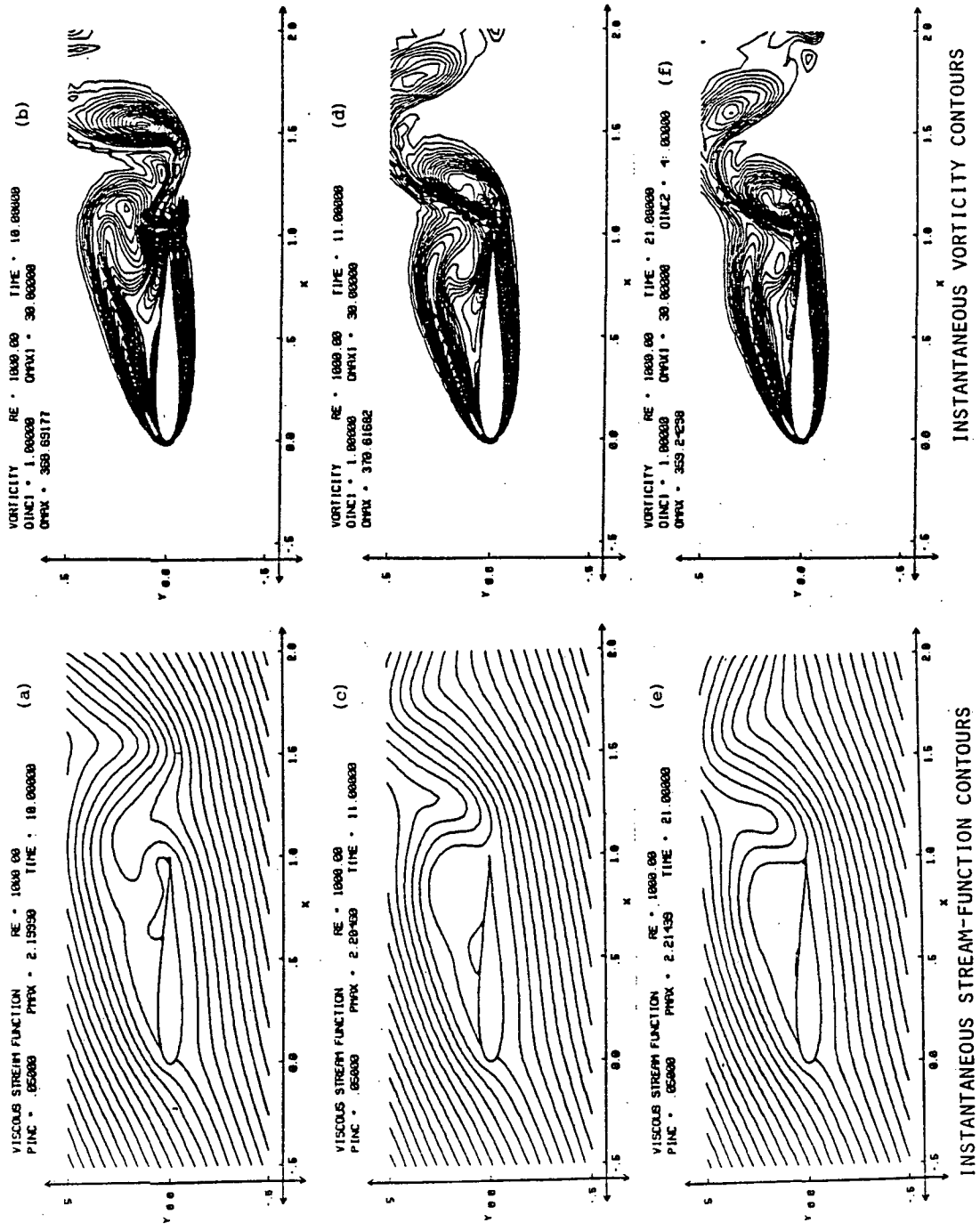

Fig. 4. Flow Past Symmetric Joukowski Airfoil at Re = 1,000, α = 15°. T = 10.00, 11.00 and 21.00.

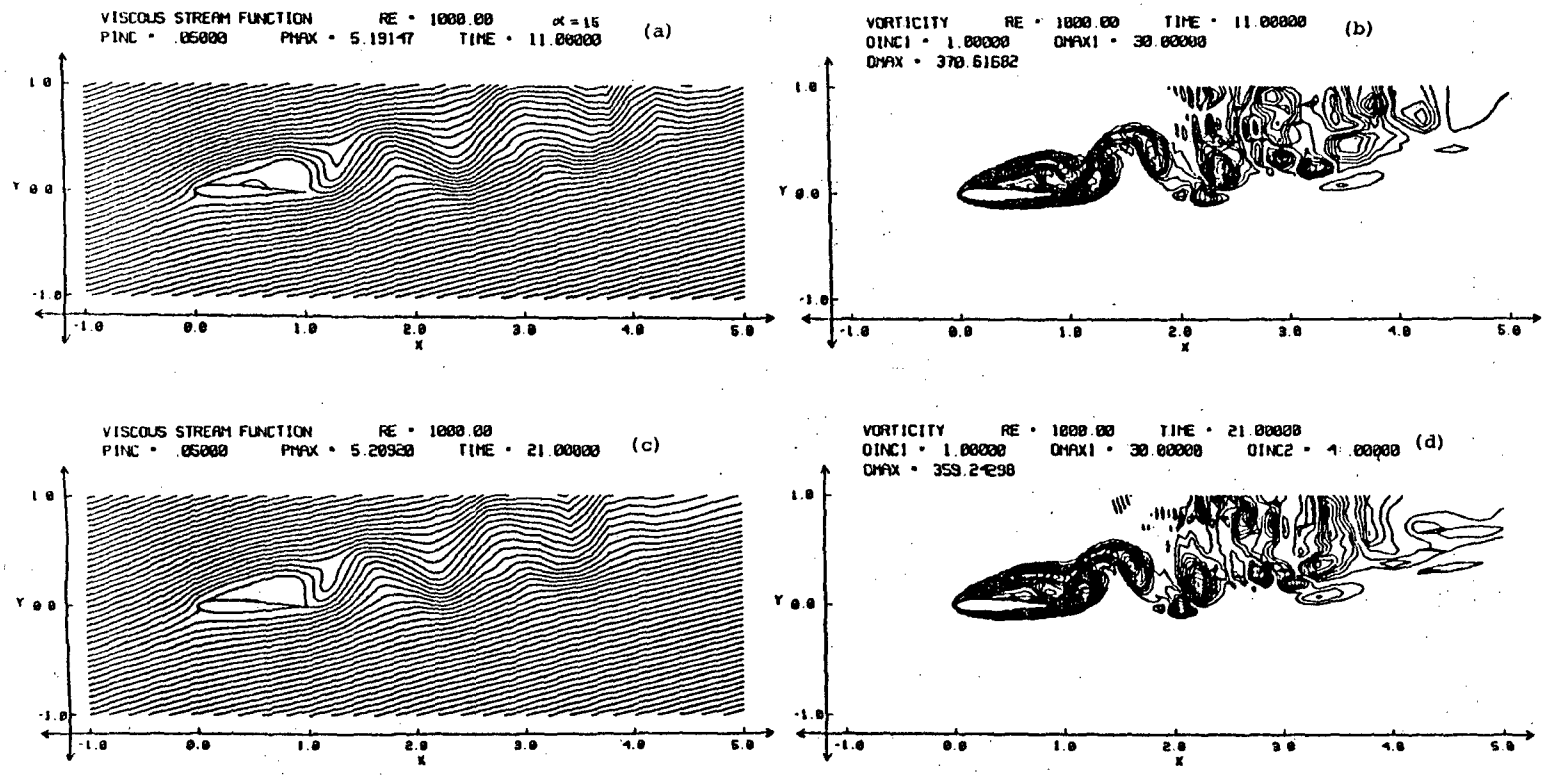

INSTANTANEOUS STREAM-FUNCTION CONTOURS

INSTANTANEOUS VORTICITY CONTOURS

Fig. 5. Flow Past Symmetric Joukowski Airfoil at Re = 1,000, α = 15°. T = 11.00 and 21.00

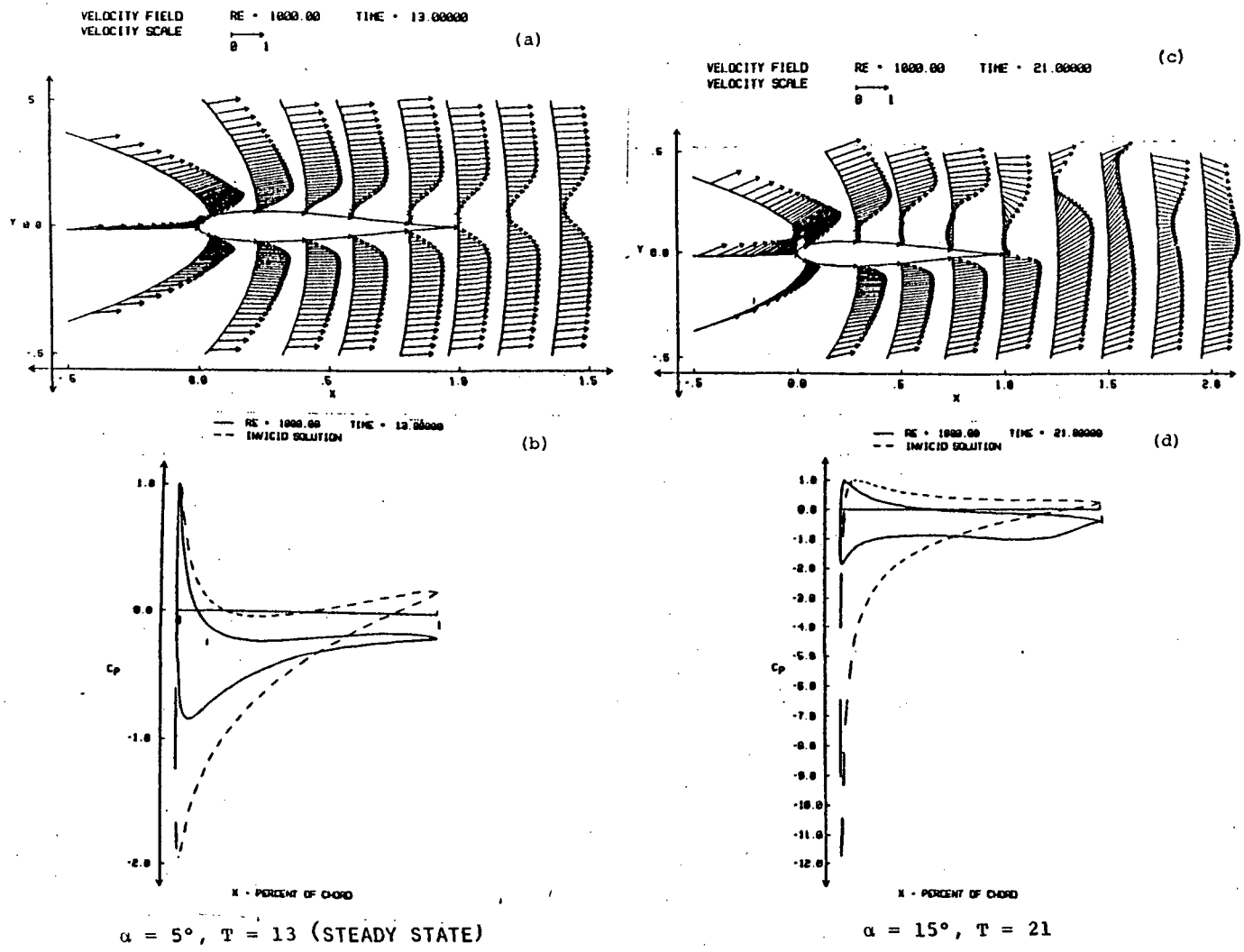

Fig. 6. Velocity Vectors and Surface Pressure Coefficient for Flow Past Symmetric Joukowski Airfoil at Incidence; Re = 1,000.

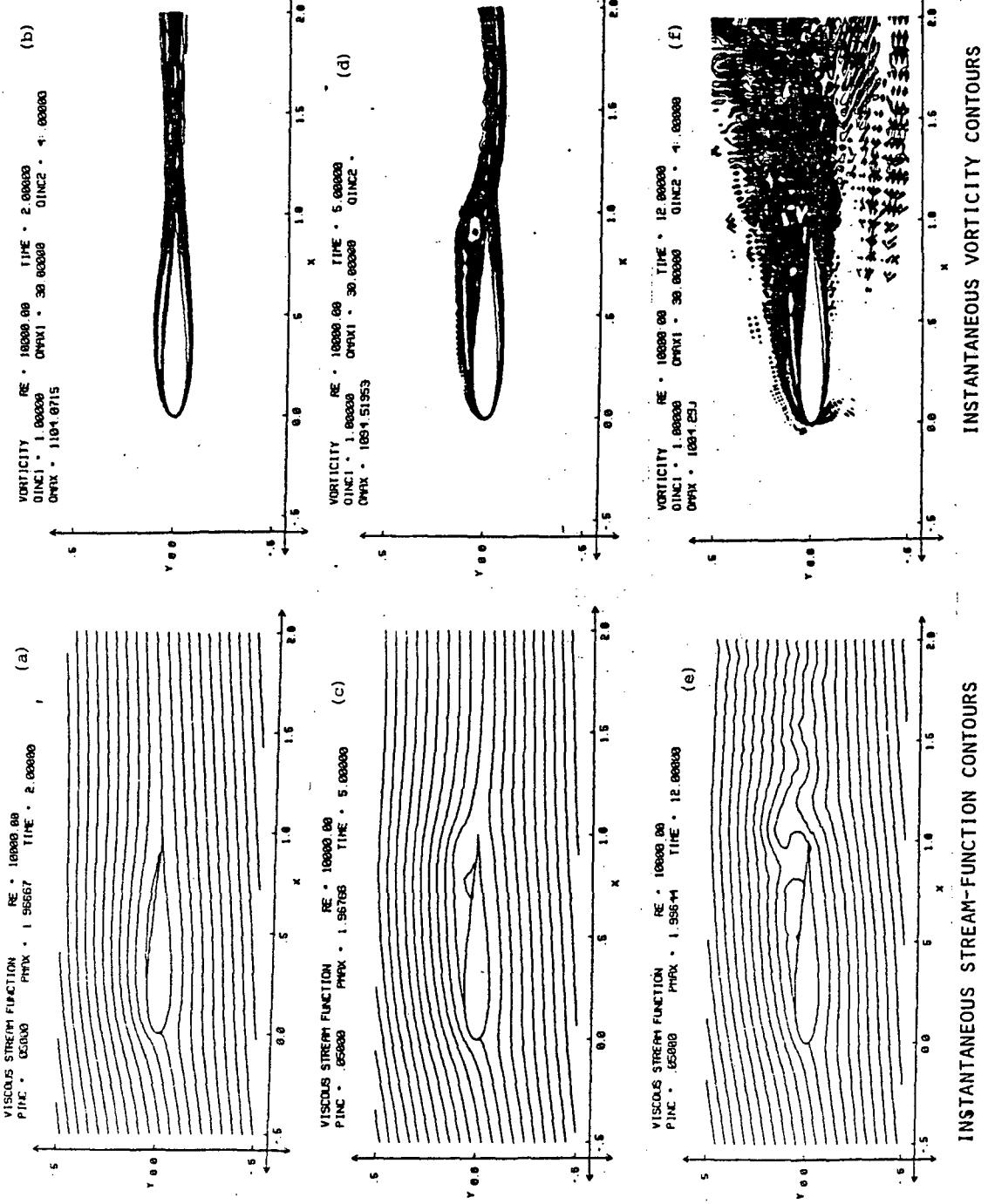

Fig. 7. Flow Past Symmetric Joukowski Airfoil at Re = 10,000, α = 5°. T = 2.00, 5.00 and 12.00.

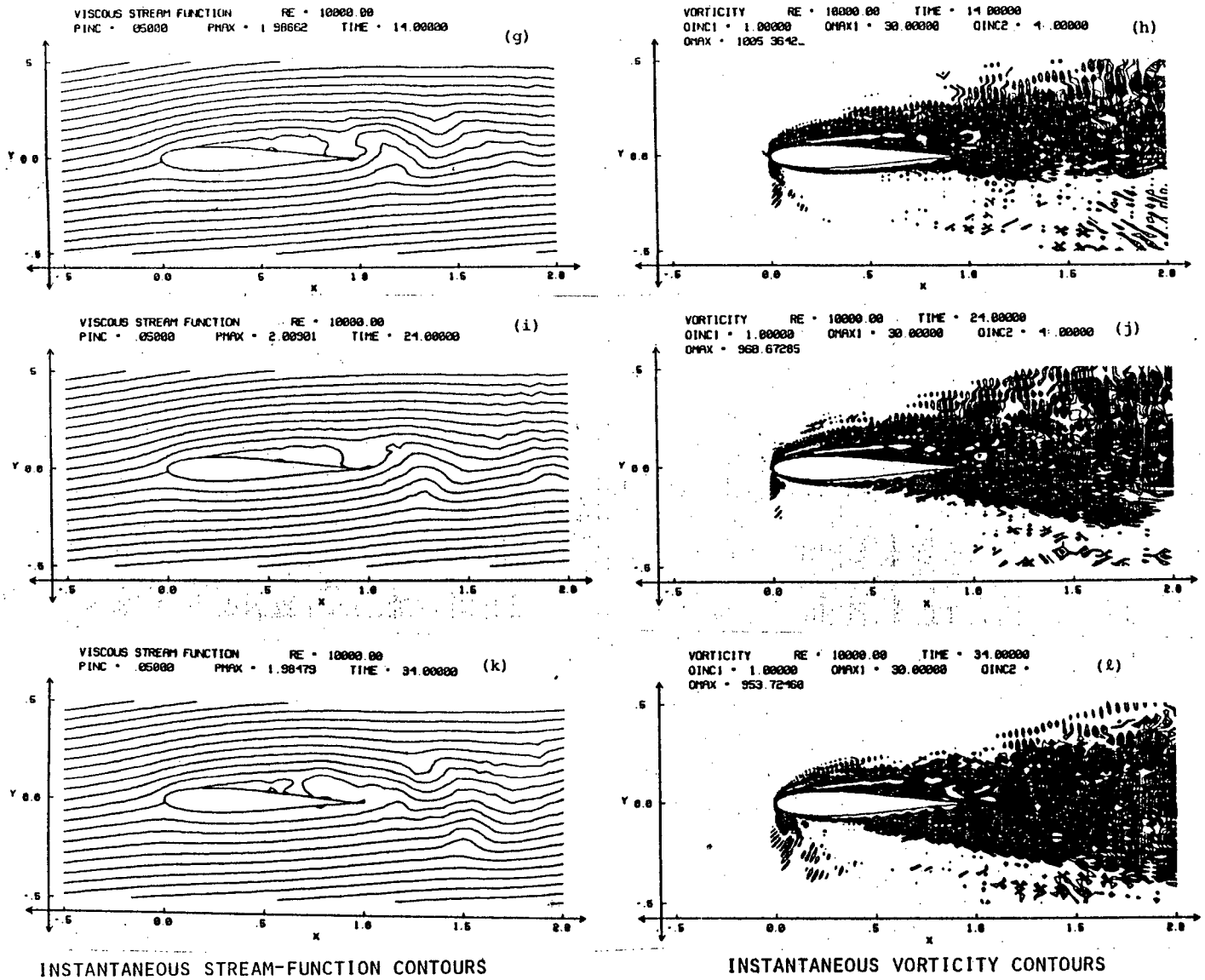

Fig. 7 (Concluded). Flow Past Symmetric Joukowski Airfoil at Re = 10,000, $\alpha = 5°$. T = 14.00, 24.00 and 34.00.